JAERI-Research
94-011

ONSET OF ELMS IN JT-60U

August 1994

Yutaka KAMADA, Masayasu SATO
Mitsuru KIKUCHI and Masahiro MORI

日本原子力研究所
Japan Atomic Energy Research Institute

本レポートは，日本原子力研究所が不定期に公刊している研究報告書です。
入手の問合わせは，日本原子力研究所技術情報部情報資料課（〒319-11 茨城県那珂郡東海村）あて，お申し越しください。なお，このほかに財団法人原子力弘済会資料センター（〒319-11 茨城県那珂郡東海村日本原子力研究所内）で複写による実費頒布をおこなっております。

This report is issued irregularly.
Inquiries about availability of the reports should be addressed to Information Division, Department of Technical Information, Japan Atomic Energy Research Institute, Tokai-mura, Naka-gun, Ibaraki-ken 319-11, Japan.

編集兼発行　日本原子力研究所
印　　刷　いばらき印刷㈱

JAERI-Research 94-011

Onset of ELMs in JT-60U

Yutaka KAMADA, Masayasu SATO, Mitsuru KIKUCHI and Masahiro MORI

Department of Fusion Plasma Research
Naka Fusion Research Establishment
Japan Atomic Energy Research Institute
Naka-machi, Naka-gun, Ibaraki-ken

(Received July 1, 1994)

The ELMs limiting the energy confinement in JT-60U appear when the heating power is high enough compared to the threshold power for the L-H transition. The ELM-free phase is observed when $\bar{n}_e$ is lower than the threshold density $\bar{n}_e^{th}$. The threshold density $\bar{n}_e^{th}$ increases with $(B_t^2/(Rq_{eff}^2))l_i$ which is a measure parameter for the ballooning stability, where q_{eff} is the effective safety factor at the edge. The edge pressure gradient estimated by $\bar{n}_e^{th}\ T_i\ (95\%)/(\ T_i\ (95\%)^{0.5}/B_p\ (a))$ is proportional to $(B_t^2/(\ Rq_{eff}^2))l_i$ which allows us to understand that the ELMs are related to the ballooning instability. A time dependent analysis of the evolution of pressure and current profiles including the bootstrap current shows that the steep edge pressure gradient is close to the marginal value for the high-n ideal ballooning instability at the onset of ELMs.

Keywords: JT-60U, ELM, MHD Instability, Ballooning Mode, H-mode

ＪＴ－60ＵにおけるＥＬＭの発生条件

日本原子力研究所那珂研究所炉心プラズマ研究所
鎌田　裕・佐藤　正泰・菊池　満・森　雅博

（1994年７月１日受理）

ＪＴ－60Ｕにおいて閉じ込め性能を制限しているＥＬＭは，加熱パワーがＨモード遷移に必要な加熱パワーしきい値に比べて十分高い場合に出現する。ＥＬＭの無いＨモード状態が得られるのは，線平均電子密度が，しきい値n_e^{th}以下の場合のみであり，これ以上の線平均電子密度ではＥＬＭのあるＨモードとなる。この密度しきい値n_e^{th}は，バルーニング不安定性の指標パラメータである$(B_t^2/(Rq_{eff}^2))l_i$の値とともに上昇する。ここで，q_{eff}はプラズマ表面での実効的安全係数である。$n_e^{th}\ T_i(95\%)/(T_i(95\%)^{0.5}/B_p(a))$で評価したプラズマ周辺部での圧力勾配は$(B_t^2/(Rq_{eff}^2))l_i$に比例する。この依存性から，ＪＴ－60ＵにおけるＥＬＭはバルーニング不安定性に起因していると理解できる。プラズマ中の圧力分布及びブートストラップ電流も含めた電流分布の時間発展を解析した結果，プラズマ周辺での急俊な圧力勾配は，高ｎの理想バルーニングモードの安定限界に近接していることがわかった。

那珂研究所：〒311－01　茨城県那珂郡那珂町大字向山801－１

Contents

目　　次

1. Introduction

To demonstrate attractiveness of tokamak fusion reactors, the following conditions should be satisfied simultaneously; high confinement improvement (high H-factor) for ignition, high normalized β (β_N) for high fusion power density, high poloidal β (β_p) for high bootstrap current fraction, short particle confinement for high purity, disruption-free for safety and dense & cold divertor condition for high efficiency of heat and particle exhaust. In this paper, the H-factor is given by the experimentally obtained energy confinement time τ_E normalized by τ_E predicted by the ITER89-P law ($H=\tau_E^{EXP}/\tau_E^{ITER89P}$) [1], β_N is defined by $\beta_t(\%)/(I_p(MA)/a(m)B_t(T))$ with the toroidal β value β_t, the plasma current I_p and the toroidal magnetic field B_t. If the above conditions are satisfied simultaneously and the absolute values of τ_E and β_t are high enough, an attractive tokamak reactor can be designed. With the recent progress of tokamak research [2], many of the above conditions have reached the reactor relevant level. However, in many cases, the attained results have satisfied only the individual condition of the above requirements. In addition, most of the good performance have been obtained transiently. For achievement of the favorable integrated performance in a steady state, the most important issue is the optimization of the MHD stability condition, because the achievement and steadiness of the above mentioned conditions are almost always prevented by the MHD instabilities.

This paper treats the onset conditions of ELMs based on the experimental results for the contribution to ITER EDA. The confinement performance achieved in the JT-60U H-mode discharges is limited by the appearance of ELMs. For the typical high plasma current at I_p~3-4MA, the poloidal magnetic field at the edge $B_p(a)$ reaches ~1T in JT-60U. The observed width of the edge pressure pedestal δ_{ped} decreases with $B_p(a)$ and δ_{ped}=2-3cm (δ_{ped}/a=3-4%) at $B_p(a)$~1T [3]. In this case, the ion temperature at the 95% of the outermost flux surface $T_i(95\%)$ is 5-7keV and a large pressure gradient is produced in the very edge region. The study on the MHD stability condition for this kind of H-mode with a large $B_p(a)$ and a small δ_{ped} is important for the design study of the future devices with a large plasma current like ITER.

Another important purpose of this paper is to study the onset conditions of ELMs at high aspect ratio A, low elongation κ and small triangularity δ, which contributes to construct the data base of effects of configuration on the edge stability condition required in the design study of future devices. The plasma configuration produced in the JT-60U H-mode experiments has high A of 3.1~4, low κ of 1.3-1.8 and small δ of 0.03-0.3, which has remarkable contrast to DIII-D (A~2.5, κ~1.7-2.1, δ~0.2-0.8). The fusion power density is proportional to the square of $\beta_N B_t^2 \varepsilon/q$. If the maximum field at the toroidal coil is limited, the fusion power density increases with increasing aspect ratio for a given β_N and q. This is because $B_t^2\varepsilon$ for a reactor may increase as the aspect ratio increases in the range of A<4-6. Therefore the study on the ELM effects on the limit of β_N at the high aspect ratio is important.

In addition, from the reactor engineering point of view, in particular for the divertor design, it is beneficial to design a single null configuration with medium triangularity to optimize the capability of the divertor tile replacement and to keep the efficient particle pumping from the inner hit point on the divertor tiles. On the other hand, from the stability point of view, it is beneficial to design a low A, high-κ and high-δ configuration for a high β operation. Therefore we should optimize the trade-off between the engineering and the stability issues in the next step devices.

2. Operational Regions of JT-60U Plasmas

From the view point of stability conditions at high β_N, the operation regions of JT-60U plasmas are categorized into three groups; the standard H-mode [4], the high-β_p mode [5] and the high β_N experiment [6,7]. The achieved values of β_N of the three gropes are given in Fig.1 as a function of q_{eff}. The effective safety factor at the edge q_{eff} is defined by [8]

$$q_{eff}=\frac{2\pi a^2 B_t}{\mu_0 R I_p}\left(\frac{1+\kappa^2}{2}\right)\left[1+\varepsilon^2\left(1+\frac{\Lambda^2}{2}\right)\right] \times [1.24 - 0.54\kappa + 0.3(\kappa^2+\delta^2) + 0.13\delta]$$

where ε is inverse aspect ratio and $\Lambda=\beta_p+l_i/2$. The safety factor at 95% of the outermost flux surface q_{95} is given by $q_{95}\sim 0.8 q_{eff}$ for the discharges in JT-60U. In the standard H-mode discharges in JT-60U, the obtained β_N-values are lower than 1.8 which is limited by onset of ELMs. In the high-β_p mode discharges, the achievable β_N-values are limited by the appearance of the β_p-collapse [5]. In the high β_N experiment the pressure driven MHD mode with low (m,n) determines the upper values of β_N [9].

The discharge parameters and the typical plasma configuration of the three gropes are given in Table 1 and Fig.2. From the stability point of view, the main differences among these gropes are the pressure and current profiles which are related to the selection of the plasma configuration relative to the injection trajectories of neutral beams (NB) and the l_i values of the target OH plasmas before NB injection. The internal inductance of the plasma column l_i is used as a measure of the shape of the current profile. That is given by

$$l_i=\left(\int B_p^2 dv/V_p\right)/\left(\mu_0 I_p/\int dl\right)^2$$

where the volume and line integrals are taken at the outermost effective flux surface given by the equilibrium calculation. Usually the values of l_i are calculated from Λ by the MHD equilibrium analysis and β_p^{dia}, where β_p^{dia} is calculated with a diamagnetic loop. In JT-60U, the selection of the plasma volume V_p and the major radius R is closely related to the heating profile of NB injection. JT-60U has 14 units of NB injectors which consist of 10 units of near perpendicular injectors, two tangential injectors parallel to the plasma current (co-tangential) and two tangential injectors anti-parallel to the plasma current (counter-tangential).

In the standard H-mode in JT-60U [4], the maximum H-factor is ~2.7 for ELM-free H-mode and ~2.0 for ELMy H-mode. The plasma configuration has relatively large volume of

In addition, from the reactor engineering point of view, in particular for the divertor design, it is beneficial to design a single null configuration with medium triangularity to optimize the capability of the divertor tile replacement and to keep the efficient particle pumping from the inner hit point on the divertor tiles. On the other hand, from the stability point of view, it is beneficial to design a low A, high-κ and high-δ configuration for a high β operation. Therefore we should optimize the trade-off between the engineering and the stability issues in the next step devices.

2. Operational Regions of JT-60U Plasmas

From the view point of stability conditions at high β_N, the operation regions of JT-60U plasmas are categorized into three groups; the standard H-mode [4], the high-β_p mode [5] and the high β_N experiment [6,7]. The achieved values of β_N of the three gropes are given in Fig.1 as a function of q_{eff}. The effective safety factor at the edge q_{eff} is defined by [8]

$$q_{eff}=\frac{2\pi a^2 B_t}{\mu_0 R I_p}\left(\frac{1+\kappa^2}{2}\right)\left[1+\varepsilon^2\left(1+\frac{\Lambda^2}{2}\right)\right] \times [1.24 - 0.54\kappa + 0.3(\kappa^2+\delta^2) + 0.13\delta]$$

where ε is inverse aspect ratio and $\Lambda=\beta_p+l_i/2$. The safety factor at 95% of the outermost flux surface q_{95} is given by $q_{95}\sim 0.8 q_{eff}$ for the discharges in JT-60U. In the standard H-mode discharges in JT-60U, the obtained β_N-values are lower than 1.8 which is limited by onset of ELMs. In the high-β_p mode discharges, the achievable β_N-values are limited by the appearance of the β_p-collapse [5]. In the high β_N experiment the pressure driven MHD mode with low (m,n) determines the upper values of β_N [9].

The discharge parameters and the typical plasma configuration of the three gropes are given in Table 1 and Fig.2. From the stability point of view, the main differences among these gropes are the pressure and current profiles which are related to the selection of the plasma configuration relative to the injection trajectories of neutral beams (NB) and the l_i values of the target OH plasmas before NB injection. The internal inductance of the plasma column l_i is used as a measure of the shape of the current profile. That is given by

$$l_i=\left(\int B_p^2 dv/V_p\right)/\left(\mu_0 I_p/\int dl\right)^2$$

where the volume and line integrals are taken at the outermost effective flux surface given by the equilibrium calculation. Usually the values of l_i are calculated from Λ by the MHD equilibrium analysis and β_p^{dia}, where β_p^{dia} is calculated with a diamagnetic loop. In JT-60U, the selection of the plasma volume V_p and the major radius R is closely related to the heating profile of NB injection. JT-60U has 14 units of NB injectors which consist of 10 units of near perpendicular injectors, two tangential injectors parallel to the plasma current (co-tangential) and two tangential injectors anti-parallel to the plasma current (counter-tangential).

In the standard H-mode in JT-60U [4], the maximum H-factor is ~2.7 for ELM-free H-mode and ~2.0 for ELMy H-mode. The plasma configuration has relatively large volume of

V_p~70-95m^3 . The produced plasmas have broad pressure profiles. In this case, confinement is limited by ELMs.

In the high β_p mode experiment, the H-factor reached up to 3.6 [10]. The key operational points are; small volume of V_p~50m^3, strong central heating with perpendicular NB, high B_t of 3-4.4T and relatively high-q_{eff} with low-l_i to avoid sawteeth in the target plasma before NB injection. The produced plasmas have highly peaked pressure profiles and broad current profiles. In this case the confinement is limited by the β_p-collapse [5] which is a pressure driven mode with medium poloidal mode numbers (m) and toroidal mode numbers (n) located in the inner region (r~0.5-0.7a) of the plasma [9].

In the high β_N experiments, we selected low B_t (1-1.5T), low I_p (0.4-0.9MA) and medium plasma volume V_p (~ 60m^3). The selected configuration in the high-β_N experiment is the intermediate configuration between the high-β_p mode and the standard H-mode. The plasmas have the pressure profile broader than that in the high-β_p mode and more peaked than that in the standard H-mode. The target l_i is typically higher than that in the other two groups. The stored energy can increase continuously even after the onset of ELMs.

In the high β_p mode and the high β_N experiments in JT-60U, the upper limit of β_N tends to increase with increasing l_i and broadening of the pressure profile [6]. The observed mode structure has clear in-out asymmetry and the fluctuation level on the good curvature side is much higher than that on the bad curvature side, which is typical for pressure driven modes. The observed mode numbers were n=1-2 and m=2-5. The obtained β-limit agrees with that of kink-ballooning mode calculated with ERATO [11]. The observed growth time of the pressure driven instabilities is in the ideal time scale for the high-β_p mode. On the other hand, the growth time is in the resistive time scale in the high-β_N experiment.

As shown above, the attainable β-values and the energy confinement in the JT-60U improved confinement experiments are limited by the MHD instabilities where the pressure driven term plays important roles and the dominant instability and its structure change with pressure and current profiles.

3. Typical Evolution of the H-mode in JT-60U

In the standard H-mode discharges in JT-60U, the plasma stored energy W^{dia} (diamagnetically measured value) continues to increase temporally in the ELM-free phase. However, W^{dia} saturates immediately after the onset of ELMs. The time evolution of the typical H-mode discharge (E16116) is shown in Fig.3. In this case, I_p=2.7MA, B_t=4T and q_{eff}=4.3. At the onset of the first ELM (t=7.95s), the edge electron temperature T_e(95%) measured by electron cyclotron emission (ECE) and the edge ion temperature T_i(98%) measured by charge exchange recombination spectroscopy (CXRS) reach ~2.8keV and ~4.5keV, respectively. The profiles of T_i, T_e and the electron density n_e at t=7.95s are shown in Fig.4. The n_e profile is estimated from the chord averaged density $\bar{n}_e$ measured by two off-axis FIR interferometers. In

V_p~70-95m^3 . The produced plasmas have broad pressure profiles. In this case, confinement is limited by ELMs.

In the high β_p mode experiment, the H-factor reached up to 3.6 [10]. The key operational points are; small volume of V_p~50m^3, strong central heating with perpendicular NB, high B_t of 3-4.4T and relatively high-q_{eff} with low-l_i to avoid sawteeth in the target plasma before NB injection. The produced plasmas have highly peaked pressure profiles and broad current profiles. In this case the confinement is limited by the β_p-collapse [5] which is a pressure driven mode with medium poloidal mode numbers (m) and toroidal mode numbers (n) located in the inner region (r~0.5-0.7a) of the plasma [9].

In the high β_N experiments, we selected low B_t (1-1.5T), low I_p (0.4-0.9MA) and medium plasma volume V_p (~ 60m^3). The selected configuration in the high-β_N experiment is the intermediate configuration between the high-β_p mode and the standard H-mode. The plasmas have the pressure profile broader than that in the high-β_p mode and more peaked than that in the standard H-mode. The target l_i is typically higher than that in the other two groups. The stored energy can increase continuously even after the onset of ELMs.

In the high β_p mode and the high β_N experiments in JT-60U, the upper limit of β_N tends to increase with increasing l_i and broadening of the pressure profile [6]. The observed mode structure has clear in-out asymmetry and the fluctuation level on the good curvature side is much higher than that on the bad curvature side, which is typical for pressure driven modes. The observed mode numbers were n=1-2 and m=2-5. The obtained β-limit agrees with that of kink-ballooning mode calculated with ERATO [11]. The observed growth time of the pressure driven instabilities is in the ideal time scale for the high-β_p mode. On the other hand, the growth time is in the resistive time scale in the high-β_N experiment.

As shown above, the attainable β-values and the energy confinement in the JT-60U improved confinement experiments are limited by the MHD instabilities where the pressure driven term plays important roles and the dominant instability and its structure change with pressure and current profiles.

3. Typical Evolution of the H-mode in JT-60U

In the standard H-mode discharges in JT-60U, the plasma stored energy W^{dia} (diamagnetically measured value) continues to increase temporally in the ELM-free phase. However, W^{dia} saturates immediately after the onset of ELMs. The time evolution of the typical H-mode discharge (E16116) is shown in Fig.3. In this case, I_p=2.7MA, B_t=4T and q_{eff}=4.3. At the onset of the first ELM (t=7.95s), the edge electron temperature T_e(95%) measured by electron cyclotron emission (ECE) and the edge ion temperature T_i(98%) measured by charge exchange recombination spectroscopy (CXRS) reach ~2.8keV and ~4.5keV, respectively. The profiles of T_i, T_e and the electron density n_e at t=7.95s are shown in Fig.4. The n_e profile is estimated from the chord averaged density $\bar{n}_e$ measured by two off-axis FIR interferometers. In

the following part of this paper, $\bar{n}_e$ represents the value of the line averaged electron density measured by the interferometer viewing r~0.4-0.5a.

An important behavior of the edge plasma in the JT-60U H-mode is that the edge temperature increases almost linearly with $\bar{n}_e$. This behavior is shown in Fig.5(a) where the data are plotted from 7.1s (NB turn-on) to 7.9s (ELM onset) for the discharge E16116. This dependence means that the edge pressure is almost proportional to $\bar{n}_e^2$. In this paper, we assume that the product $\bar{n}_e(0.4\text{-}0.5a)T_i(95\%)$ represents the edge pressure. Figure 5(b) shows the evolution of the discharge on the $\bar{n}_e(0.4\text{-}0.5a)T_i(95\%)$-$l_i$ plane. With the evolution of H-mode, l_i decreases and $\bar{n}_eT_i(95\%)$ increases, and the first ELM appears at $\bar{n}_eT_i(95\%)\sim11\times10^{19}m^{-3}keV$.

4. Onset Conditions of ELMs

In JT-60U, ELMs seem to be categorized into two gropes. The first one appears when the absorbed heating power is high enough compared to the threshold heating power required for the L-H transition P_{abs}^{th}. The other type sometimes appears when the absorbed power is close to P_{abs}^{th}. Figure 6(a) shows the ELM frequency f_{ELM} against absorbed NB power P_{NB}^{abs} for B_t=2T (closed circles) and 3T (open circles) with the plasma volume V_p=82-88m^3. The threshold power P_{abs}^{th} for the L-H transition is indicated by dashed lines. Both open and closed circles increase almost linearly with P_{NB}^{abs} if P_{NB}^{abs} is high enough. On the other hand, if P_{NB}^{abs} is close to P_{abs}^{th}, there is another group with high f_{ELM}. In Fig.6(b), where f_{ELM} is plotted against $(P_{NB}^{abs})/((B_t^2/(Rq_{eff}^2))l_i)$, f_{ELM} increases linearly with $(P_{NB}^{abs})/((B_t^2/(Rq_{eff}^2))l_i$) in the first group. In the second group, f_{ELM} is high even at low P_{NB}^{abs}. The separation suggests that the origin of the ELM activity can be categorized into two types. The parameter $(B_t^2/(Rq_{eff}^2))l_i$ is a measure parameter for the ballooning instability. Later in this section, we will show that the parameter $(B_t^2/(Rq_{eff}^2))l_i$ can be a good measure to discuss the onset condition of ELMs.

The ELMs limiting the energy confinement in JT-60U appear when the heating power is high enough as shown in Fig.6. In the following part, we discuss the onset condition of this kind of ELMs. The discharge parameters are; I_p=0.7-3.5MA, B_t=1.5-4T, V_p=60-75m^3 and κ=1.55-1.7.

In JT-60U, the ELM-free phase is observed only when $\bar{n}_e$ is lower than the threshold value $\bar{n}_e^{th}$. If $\bar{n}_e$ is higher than $\bar{n}_e^{th}$, the discharge becomes ELMy H-mode. Figure 7(a) shows $\bar{n}_e^{th}$ increases clearly with I_p. To understand this dependence, we use the parameter $(B_t^2/(Rq_{eff}^2))l_i$ which is a measure parameter for pressure driven instabilities. This parameter is nearly proportional to $I_p^2l_i$ for a fixed plasma configuration. Although, for a correct treatment, the edge magnetic shear should be used instead of l_i, the direct measurement of the edge shear has not been available in JT-60U. Therefore, we use l_i as a measure of the magnetic shear. Figure 7(b) shows the relationship between $\bar{n}_e^{th}$ and $(B_t^2/(Rq_{eff}^2))l_i$. We can observe a clear relationship between $\bar{n}_e^{th}$ and $(B_t^2/(Rq_{eff}^2))l_i$. In Fig.7, the open circles indicate the data

the following part of this paper, $\bar{n}_c$ represents the value of the line averaged electron density measured by the interferometer viewing r~0.4-0.5a.

An important behavior of the edge plasma in the JT-60U H-mode is that the edge temperature increases almost linearly with $\bar{n}_e$. This behavior is shown in Fig.5(a) where the data are plotted from 7.1s (NB turn-on) to 7.9s (ELM onset) for the discharge E16116. This dependence means that the edge pressure is almost proportional to $\bar{n}_e^2$. In this paper, we assume that the product $\bar{n}_e(0.4\text{-}0.5a)T_i(95\%)$ represents the edge pressure. Figure 5(b) shows the evolution of the discharge on the $\bar{n}_e(0.4\text{-}0.5a)T_i(95\%)$-$l_i$ plane. With the evolution of H-mode, l_i decreases and $\bar{n}_eT_i(95\%)$ increases, and the first ELM appears at $\bar{n}_eT_i(95\%)\sim11\times10^{19}m^{-3}keV$.

4. Onset Conditions of ELMs

In JT-60U, ELMs seem to be categorized into two gropes. The first one appears when the absorbed heating power is high enough compared to the threshold heating power required for the L-H transition P_{abs}^{th}. The other type sometimes appears when the absorbed power is close to P_{abs}^{th}. Figure 6(a) shows the ELM frequency f_{ELM} against absorbed NB power P_{NB}^{abs} for B_t=2T (closed circles) and 3T (open circles) with the plasma volume V_p=82-88m^3. The threshold power P_{abs}^{th} for the L-H transition is indicated by dashed lines. Both open and closed circles increase almost linearly with P_{NB}^{abs} if P_{NB}^{abs} is high enough. On the other hand, if P_{NB}^{abs} is close to P_{abs}^{th}, there is another group with high f_{ELM}. In Fig.6(b), where f_{ELM} is plotted against $(P_{NB}^{abs})/((B_t^2/(Rq_{eff}^2))l_i)$, f_{ELM} increases linearly with $(P_{NB}^{abs})/((B_t^2/(Rq_{eff}^2))l_i$) in the first group. In the second group, f_{ELM} is high even at low P_{NB}^{abs}. The separation suggests that the origin of the ELM activity can be categorized into two types. The parameter $(B_t^2/(Rq_{eff}^2))l_i$ is a measure parameter for the ballooning instability. Later in this section, we will show that the parameter $(B_t^2/(Rq_{eff}^2))l_i$ can be a good measure to discuss the onset condition of ELMs.

The ELMs limiting the energy confinement in JT-60U appear when the heating power is high enough as shown in Fig.6. In the following part, we discuss the onset condition of this kind of ELMs. The discharge parameters are; I_p=0.7-3.5MA, B_t=1.5-4T, V_p=60-75m^3 and κ=1.55-1.7.

In JT-60U, the ELM-free phase is observed only when $\bar{n}_e$ is lower than the threshold value $\bar{n}_e^{th}$. If $\bar{n}_e$ is higher than $\bar{n}_e^{th}$, the discharge becomes ELMy H-mode. Figure 7(a) shows $\bar{n}_e^{th}$ increases clearly with I_p. To understand this dependence, we use the parameter $(B_t^2/(Rq_{eff}^2))l_i$ which is a measure parameter for pressure driven instabilities. This parameter is nearly proportional to $I_p^2l_i$ for a fixed plasma configuration. Although, for a correct treatment, the edge magnetic shear should be used instead of l_i, the direct measurement of the edge shear has not been available in JT-60U. Therefore, we use l_i as a measure of the magnetic shear. Figure 7(b) shows the relationship between $\bar{n}_e^{th}$ and $(B_t^2/(Rq_{eff}^2))l_i$. We can observe a clear relationship between $\bar{n}_e^{th}$ and $(B_t^2/(Rq_{eff}^2))l_i$. In Fig.7, the open circles indicate the data

taken in a wide range of I_p (0.7-3.5MA) and B_t (1.5-4T) and closed circles correspond to the data for a fixed $B_t^2/(Rq_{eff}^2)$ (=0.08-0.11; 1.5MA, 3T). The behavior of the closed circles indicates that $\bar{n}_e^{th}$ increases with l_i even when B_t and I_p are fixed [12].

In Fig.7(c), $\bar{n}_e(0.4\text{-}0.5a)T_i(95\%)$ (a measure of the edge pressure) is plotted against $(B_t^2/(Rq_{eff}^2))l_i$. The edge pressure limit at the onset of ELMs seems to increase with $(B_t^2/(Rq_{eff}^2))l_i$. In the JT-60U H-mode, the width of pressure pedestal δ_{ped} is proportional to the poloidal Larmor radius of thermal ions [3] which scales with $(T_i(95\%)^{0.5}/B_p(a))$. Therefore we can assume the edge pressure gradient is proportional to $(\bar{n}_e^{th}T_i(95\%))/(T_i(95\%)^{0.5}/B_p(a))$ (~(edge pressure)/δ_{ped}). In Fig.7(d), $(\bar{n}_e^{th}T_i(95\%))/(T_i(95\%)^{0.5}/B_p(a))$ is clearly proportional to $(B_t^2/(Rq_{eff}^2))l_i$. This result implies that the edge pressure gradient is a function of $(B_t^2/(Rq_{eff}^2))l_i$ and that the ELMs are related to the ballooning instability. Concerning the usual s-α diagram for the high-n ideal ballooning mode, both the clear proportionality in Fig.7(d) and evolution on the l_i-$\bar{n}_e^{th}T_i(95\%)$ plane in Fig.5(b) suggest that the edge plasmas in JT-60U H-mode are in the first stability regime.

The data of $n_e(95\%)$ and $n_e(95\%)T_i(95\%)$ for the VH-mode in DIIID and JET reported in Ref.[13] are plotted in Figs.7(a) and 7(c) for comparison. In these VH-mode discharges, $n_e(95\%)$ and $n_e(95\%)T_i(95\%)$ are not limited by appearance of ELMs and Ref.[13] suggests that the second stable regime for the ideal ballooning mode is accessible with a large triangularity in DIIID and a large edge bootstrap current in JET. Although, from Fig.7(c), the edge pressure of the JT-60U H-mode discharges is in the same range compared to these VH mode discharges, the edge pressure is limited by ELMs and the edge plasma seems to be in the first regime for the ideal ballooning mode.

5. Time Dependent Analysis for High-n Ideal Ballooning Stability

According to the analysis shown in Sec.4, the ballooning mode seems to cause the onset of ELMs. However, for more detailed discussions, the time dependent analysis including the evolution of the current profile is required. In particular, the steep pressure gradient at the edge can drive bootstrap current and the effect of the skin current on the stability condition cannot be neglected.

Figure 8 shows the evolution of the bootstrap current and the stability condition of the high-n ideal ballooning mode for the discharge E16116. The evolution was calculated with a 1.5D time dependent analysis code TOPICS. As shown in Fig.8(a), from t=7.1s (NB turn on) to 7.9s (ELM onset), th amount of the bootstrap current increases almost linearly up to 0.56MA which is 21% of the total plasma current (2.7MA). The profile of the bootstrap current is highly peaked in the edge region (Fig.8(b)) and the bootstrap current density at the edge becomes ~0.4-0.45MA/m^2 at t=7.8-8.0s which is comparable to the averaged total current density of 0.77MA/m^2 (=2.7MA/3.5m^2). In Fig.8(c), open squares and open circles correspond to -dp/dψ at ρ=0.98 and ρ=1, respectively. The critical pressure gradient for the

taken in a wide range of I_p (0.7-3.5MA) and B_t (1.5-4T) and closed circles correspond to the data for a fixed $B_t^2/(Rq_{eff}^2)$ (=0.08-0.11; 1.5MA, 3T). The behavior of the closed circles indicates that $\bar{n}_e^{th}$ increases with l_i even when B_t and I_p are fixed [12].

In Fig.7(c), $\bar{n}_e(0.4\text{-}0.5a)T_i(95\%)$ (a measure of the edge pressure) is plotted against $(B_t^2/(Rq_{eff}^2))l_i$. The edge pressure limit at the onset of ELMs seems to increase with $(B_t^2/(Rq_{eff}^2))l_i$. In the JT-60U H-mode, the width of pressure pedestal δ_{ped} is proportional to the poloidal Larmor radius of thermal ions [3] which scales with $(T_i(95\%)^{0.5}/B_p(a))$. Therefore we can assume the edge pressure gradient is proportional to $(\bar{n}_e^{th}T_i(95\%))/(T_i(95\%)^{0.5}/B_p(a))$ (~(edge pressure)/δ_{ped}). In Fig.7(d), $(\bar{n}_e^{th}T_i(95\%))/(T_i(95\%)^{0.5}/B_p(a))$ is clearly proportional to $(B_t^2/(Rq_{eff}^2))l_i$. This result implies that the edge pressure gradient is a function of $(B_t^2/(Rq_{eff}^2))l_i$ and that the ELMs are related to the ballooning instability. Concerning the usual s-α diagram for the high-n ideal ballooning mode, both the clear proportionality in Fig.7(d) and evolution on the l_i-$\bar{n}_e^{th}T_i(95\%)$ plane in Fig.5(b) suggest that the edge plasmas in JT-60U H-mode are in the first stability regime.

The data of $n_e(95\%)$ and $n_e(95\%)T_i(95\%)$ for the VH-mode in DIIID and JET reported in Ref.[13] are plotted in Figs.7(a) and 7(c) for comparison. In these VH-mode discharges, $n_e(95\%)$ and $n_e(95\%)T_i(95\%)$ are not limited by appearance of ELMs and Ref.[13] suggests that the second stable regime for the ideal ballooning mode is accessible with a large triangularity in DIIID and a large edge bootstrap current in JET. Although, from Fig.7(c), the edge pressure of the JT-60U H-mode discharges is in the same range compared to these VH mode discharges, the edge pressure is limited by ELMs and the edge plasma seems to be in the first regime for the ideal ballooning mode.

5. Time Dependent Analysis for High-n Ideal Ballooning Stability

According to the analysis shown in Sec.4, the ballooning mode seems to cause the onset of ELMs. However, for more detailed discussions, the time dependent analysis including the evolution of the current profile is required. In particular, the steep pressure gradient at the edge can drive bootstrap current and the effect of the skin current on the stability condition cannot be neglected.

Figure 8 shows the evolution of the bootstrap current and the stability condition of the high-n ideal ballooning mode for the discharge E16116. The evolution was calculated with a 1.5D time dependent analysis code TOPICS. As shown in Fig.8(a), from t=7.1s (NB turn on) to 7.9s (ELM onset), th amount of the bootstrap current increases almost linearly up to 0.56MA which is 21% of the total plasma current (2.7MA). The profile of the bootstrap current is highly peaked in the edge region (Fig.8(b)) and the bootstrap current density at the edge becomes ~0.4-0.45MA/m^2 at t=7.8-8.0s which is comparable to the averaged total current density of 0.77MA/m^2 (=2.7MA/3.5m^2). In Fig.8(c), open squares and open circles correspond to -dp/dψ at ρ=0.98 and ρ=1, respectively. The critical pressure gradient for the

high-n ballooning stability at ρ=0.98 and ρ=1 are shown by + and x, respectively. The evolution of the edge stability condition shows that the steep edge pressure gradient is close to the marginal value for the high-n ideal ballooning instability at t=7.8-8.0s, which is the timing of onset of ELMs (t=7.95s). The profiles of the measured pressure gradient and the critical pressure gradient for the ballooning stability are given in Fig.8(d). The solid line with open square and the dotted line are the critical pressure gradient with and without the bootstrap current. The measured pressure gradient (solid line with closed circles) reaches the critical value at the edge. Although the edge bootstrap current tends to improve the critical pressure gradient, the measured pressure gradient at the edge still exceeds the critical value in this calculation. The stability calculation at the very edge involves uncertainty of the measurements of edge density and temperature and also uncertainty due to the high energy component. The accuracy of the equilibrium reconstruction at the edge is to be improved. Therefore we cannot conclude that the edge pressure gradient really violate the stability condition. However, we can conclude that the edge pressure gradient is close to the marginal value for the high-n ideal ballooning instability.

6. Discussion

We conclude that the linear relation between the edge pressure gradient and the ballooning parameter $(B_t^2/(Rq_{eff}^2))l_i$ shown in Fig.7(d) suggests that the ballooning instability triggers ELMs. However, the mode number has not been determined experimentally by magnetic probes, soft X ray and ECE polycrometer data. It is important to identify whether the mode is purely high-n or some low m/n mode is coupled. It is also important to clarify the kink mode stability. Although many of these issues are expected to be clarified in the future experiments, the present JT-60U data suggest that ELMs can be related to the medium or low m/n modes in some cases. Figure 9 shows the tangent of the data in Fig.7(d) ($(\bar{n}_e^{th}T_i(95\%))/(T_i(95\%)^{0.5}/B_p(a))) / (B_t^2/(Rq_{eff}^2))l_i$)) as a function of q_{eff}. In many cases, the values are nearly constant in a wide range of q_{eff}, which suggests that the many of ELMs in JT-60U are caused by the high-(m,n) mode. However, if we follow only the lower boundary of the data, we can observe fine structure depending on q_{eff} in particular when q_{eff} is around integer. This observation may suggests a possibility that some ELMs are related to the instabilities with medium or low (m,n).

The configuration of JT-60U discharges has a small triangularity (δ~0.03-0.3) which may prevent the access to the second stability regime. A modification in the connection of the poloidal windings to increase δ is under discussion in JT-60U. This modification will improve the understanding of the edge stability for the pressure and current driven instabilities.

high-n ballooning stability at ρ=0.98 and ρ=1 are shown by + and x, respectively. The evolution of the edge stability condition shows that the steep edge pressure gradient is close to the marginal value for the high-n ideal ballooning instability at t=7.8-8.0s, which is the timing of onset of ELMs (t=7.95s). The profiles of the measured pressure gradient and the critical pressure gradient for the ballooning stability are given in Fig.8(d). The solid line with open square and the dotted line are the critical pressure gradient with and without the bootstrap current. The measured pressure gradient (solid line with closed circles) reaches the critical value at the edge. Although the edge bootstrap current tends to improve the critical pressure gradient, the measured pressure gradient at the edge still exceeds the critical value in this calculation. The stability calculation at the very edge involves uncertainty of the measurements of edge density and temperature and also uncertainty due to the high energy component. The accuracy of the equilibrium reconstruction at the edge is to be improved. Therefore we cannot conclude that the edge pressure gradient really violate the stability condition. However, we can conclude that the edge pressure gradient is close to the marginal value for the high-n ideal ballooning instability.

6. Discussion

We conclude that the linear relation between the edge pressure gradient and the ballooning parameter $(B_t^2/(Rq_{eff}^2))l_i$ shown in Fig.7(d) suggests that the ballooning instability triggers ELMs. However, the mode number has not been determined experimentally by magnetic probes, soft X ray and ECE polycrometer data. It is important to identify whether the mode is purely high-n or some low m/n mode is coupled. It is also important to clarify the kink mode stability. Although many of these issues are expected to be clarified in the future experiments, the present JT-60U data suggest that ELMs can be related to the medium or low m/n modes in some cases. Figure 9 shows the tangent of the data in Fig.7(d) ($(\bar{n}_e^{th}T_i(95\%))/(T_i(95\%)^{0.5}/B_p(a))) / (B_t^2/(Rq_{eff}^2))l_i$)) as a function of q_{eff}. In many cases, the values are nearly constant in a wide range of q_{eff}, which suggests that the many of ELMs in JT-60U are caused by the high-(m,n) mode. However, if we follow only the lower boundary of the data, we can observe fine structure depending on q_{eff} in particular when q_{eff} is around integer. This observation may suggests a possibility that some ELMs are related to the instabilities with medium or low (m,n).

The configuration of JT-60U discharges has a small triangularity (δ~0.03-0.3) which may prevent the access to the second stability regime. A modification in the connection of the poloidal windings to increase δ is under discussion in JT-60U. This modification will improve the understanding of the edge stability for the pressure and current driven instabilities.

7. Summary

The ELMs limiting the energy confinement in JT-60U appears when the heating power is high enough compared to the threshold power for the L-H transition. The ELM-free phase is observed when $\bar{n}_e$ is lower than the threshold value $\bar{n}_e^{th}$. The threshold value $\bar{n}_e^{th}$ increases with $(B_t^2/(Rq_{eff}^2))l_i$ which is a measure parameter for the ballooning stability. The edge pressure gradient estimated by $\bar{n}_e^{th}T_i(95\%)/(T_i(95\%)^{0.5}/B_p(a))$ is proportional to $(B_t^2/(Rq_{eff}^2))l_i$ which can be interpreted that the ELMs are related to the ballooning instability. A time dependent analysis of the evolution of pressure and current profiles including the bootstrap current shows that the steep edge pressure gradient is close to the marginal value for the high-n ideal ballooning instability at the onset of ELMs.

Acknowledgement

The authors wish to thank Drs. M. Azumi, S. Tokuda and T. Ozeki for the development of the analyses codes and detailed discussion on the MHD stability. They also thank the members of the H-mode and MHD research groups in JT-60U. This paper has been provided for contribution to ITER EDA by responding to ITER JCT, San Diego.

References

[1] UCKAN, N.A., YUSHMANOV, P.N., TAKIZUKA, T., BORRASS, K., CALLEN, J.D., et al., in Plasma Physics and Controlled Nuclear Fusion Research. Proc.13th Int. Conf.,Washington, 1990, (IAEA, Vienna, 1991), Vol. III, p.307.

[2] see papers of the summary session in n Plasma Physics and Controlled Nuclear Fusion Research. Proc.14th Int. Conf.,Wurzburg, 1992, (IAEA, Vienna, 1993)

[3] KIKUCHI, M., et al., 1993 Proc. 20th European Conf. on Controlled Fusion and Plasma Physics (Lisboa 1993) pt I (Geneva:EPS) p179

[4] KIKUCHI, M., SHIRAI, H., TAKIZUKA, T., KAMADA, Y., KOIDE, Y., et al, in Plasma Physics and Controlled Nuclear Fusion Research. Proc.14th Int. Conf.,Wurzburg, 1992, (IAEA, Vienna, 1993), Vol.I. p.189.

[5] ISHIDA, S., MATSUOKA, M., KIKUCHI, M., TSUJI, S., NISHITANI, T., et al , in Plasma Physics and Controlled Nuclear Fusion Research. Proc.14th Int. Conf.,Wurzburg, 1992, (IAEA, Vienna, 1993), Vol.I., p.219.

[6] KAMADA, Y., et al., 'Noninductively Current Driven H-mode woth High-βN and High-βp values in JT-60U' Submitted to Nucl. Fusion.

[7] KAMADA, Y., et al., 'ELMy H-mode with high-βN and high-βp in JT-60U' to appear in Plasma Physics and Controlled Fusion.

[8] TODD,T,N., in *Proc. Second Europ. Tokamak Programme Work-shop,* Sault-Les-Chartreux, 1983, European Physical Society (1983) 123.

7. Summary

The ELMs limiting the energy confinement in JT-60U appears when the heating power is high enough compared to the threshold power for the L-H transition. The ELM-free phase is observed when $\bar{n}_e$ is lower than the threshold value $\bar{n}_e^{th}$. The threshold value $\bar{n}_e^{th}$ increases with $(B_t^2/(Rq_{eff}^2))l_i$ which is a measure parameter for the ballooning stability. The edge pressure gradient estimated by $\bar{n}_e^{th}T_i(95\%)/(T_i(95\%)^{0.5}/B_p(a))$ is proportional to $(B_t^2/(Rq_{eff}^2))l_i$ which can be interpreted that the ELMs are related to the ballooning instability. A time dependent analysis of the evolution of pressure and current profiles including the bootstrap current shows that the steep edge pressure gradient is close to the marginal value for the high-n ideal ballooning instability at the onset of ELMs.

Acknowledgement

The authors wish to thank Drs. M. Azumi, S. Tokuda and T. Ozeki for the development of the analyses codes and detailed discussion on the MHD stability. They also thank the members of the H-mode and MHD research groups in JT-60U. This paper has been provided for contribution to ITER EDA by responding to ITER JCT, San Diego.

References

[1] UCKAN, N.A., YUSHMANOV, P.N., TAKIZUKA, T., BORRASS, K., CALLEN, J.D., et al., in Plasma Physics and Controlled Nuclear Fusion Research. Proc.13th Int. Conf.,Washington, 1990, (IAEA, Vienna, 1991), Vol. III, p.307.

[2] see papers of the summary session in n Plasma Physics and Controlled Nuclear Fusion Research. Proc.14th Int. Conf.,Wurzburg, 1992, (IAEA, Vienna, 1993)

[3] KIKUCHI, M., et al., 1993 Proc. 20th European Conf. on Controlled Fusion and Plasma Physics (Lisboa 1993) pt I (Geneva:EPS) p179

[4] KIKUCHI, M., SHIRAI, H., TAKIZUKA, T., KAMADA, Y., KOIDE, Y., et al, in Plasma Physics and Controlled Nuclear Fusion Research. Proc.14th Int. Conf.,Wurzburg, 1992, (IAEA, Vienna, 1993), Vol.I. p.189.

[5] ISHIDA, S., MATSUOKA, M., KIKUCHI, M., TSUJI, S., NISHITANI, T., et al , in Plasma Physics and Controlled Nuclear Fusion Research. Proc.14th Int. Conf.,Wurzburg, 1992, (IAEA, Vienna, 1993), Vol.I., p.219.

[6] KAMADA, Y., et al., 'Noninductively Current Driven H-mode woth High-βN and High-βp values in JT-60U' Submitted to Nucl. Fusion.

[7] KAMADA, Y., et al., 'ELMy H-mode with high-βN and high-βp in JT-60U' to appear in Plasma Physics and Controlled Fusion.

[8] TODD,T,N., in *Proc. Second Europ. Tokamak Programme Work-shop,* Sault-Les-Chartreux, 1983, European Physical Society (1983) 123.

7. Summary

The ELMs limiting the energy confinement in JT-60U appears when the heating power is high enough compared to the threshold power for the L-H transition. The ELM-free phase is observed when $\bar{n}_e$ is lower than the threshold value $\bar{n}_e^{th}$. The threshold value $\bar{n}_e^{th}$ increases with $(B_t^2/(Rq_{eff}^2))l_i$ which is a measure parameter for the ballooning stability. The edge pressure gradient estimated by $\bar{n}_e^{th}T_i(95\%)/(T_i(95\%)^{0.5}/B_p(a))$ is proportional to $(B_t^2/(Rq_{eff}^2))l_i$ which can be interpreted that the ELMs are related to the ballooning instability. A time dependent analysis of the evolution of pressure and current profiles including the bootstrap current shows that the steep edge pressure gradient is close to the marginal value for the high-n ideal ballooning instability at the onset of ELMs.

Acknowledgement

The authors wish to thank Drs. M. Azumi, S. Tokuda and T. Ozeki for the development of the analyses codes and detailed discussion on the MHD stability. They also thank the members of the H-mode and MHD research groups in JT-60U. This paper has been provided for contribution to ITER EDA by responding to ITER JCT, San Diego.

References

[1] UCKAN, N.A., YUSHMANOV, P.N., TAKIZUKA, T., BORRASS, K., CALLEN, J.D., et al., in Plasma Physics and Controlled Nuclear Fusion Research. Proc.13th Int. Conf.,Washington, 1990, (IAEA, Vienna, 1991), Vol. III, p.307.

[2] see papers of the summary session in n Plasma Physics and Controlled Nuclear Fusion Research. Proc.14th Int. Conf.,Wurzburg, 1992, (IAEA, Vienna, 1993)

[3] KIKUCHI, M., et al., 1993 Proc. 20th European Conf. on Controlled Fusion and Plasma Physics (Lisboa 1993) pt I (Geneva:EPS) p179

[4] KIKUCHI, M., SHIRAI, H., TAKIZUKA, T., KAMADA, Y., KOIDE, Y., et al, in Plasma Physics and Controlled Nuclear Fusion Research. Proc.14th Int. Conf.,Wurzburg, 1992, (IAEA, Vienna, 1993), Vol.I. p.189.

[5] ISHIDA, S., MATSUOKA, M., KIKUCHI, M., TSUJI, S., NISHITANI, T., et al , in Plasma Physics and Controlled Nuclear Fusion Research. Proc.14th Int. Conf.,Wurzburg, 1992, (IAEA, Vienna, 1993), Vol.I., p.219.

[6] KAMADA, Y., et al., 'Noninductively Current Driven H-mode woth High-βN and High-βp values in JT-60U' Submitted to Nucl. Fusion.

[7] KAMADA, Y., et al., 'ELMy H-mode with high-βN and high-βp in JT-60U' to appear in Plasma Physics and Controlled Fusion.

[8] TODD,T,N., in *Proc. Second Europ. Tokamak Programme Work-shop,* Sault-Les-Chartreux, 1983, European Physical Society (1983) 123.

[9] NEYATANI, Y., et al., 1993 Proc. 20th European Conf. on Controlled Fusion and Plasma Physics (Lisboa 1993) pt I (Geneva:EPS) p215.

[10] MORI, M., et al., to appear in Nucl. Fusion.

[11] OZEKI, T., et al., to be submitted to Nucl. Fusion.

[12] KAMADA Y., TAKIZUKA, T., KIKUCHI, M., et al., in Plasma Physics and Controlled Nuclear Fusion Research. Proc.14th Int. Conf.,Wurzburg, 1992, (IAEA, Vienna, 1993) Vol. I, p.507.

[13] GREENFIELD C. M., et al., Plasma Phys. Cont. Fusion **35** (1993) B263.

Table 1 Typical Plasma Parameters
of the NB heated JT-60U plasmas

	Standard H-mode	High-β_N Experiment	High-β_p mode
I_p (MA)	0.7-3.5	0.4-0.9	0.6-2.5
B_t (T)	2-4.2	1-1.5	3-4.4
q_{eff}	2.2-12	4-15	4-14
V_p (m^3)	70-95	~60	40-50
n_e ($10^{19}m^{-3}$)	1-5	1-1.5	0.7-3
k	1.3-1.8	1.4-1.7	1.5-1.8
δ	0.03-0.3	0.15-0.25	0.05-0.15
ε	0.26-0.32	~0.25	0.22-0.25
P_{NB} perp (MW)	<34	<20	<36
P_{NB} Co-para (MW)	<5	< 4	<5
NB Heating	off-axis	off-axis	on-axis
β_N	<1.8	< 4.2	<2.5
β_p	<2.2	< 4.7	<2.9
β_t (%)	<1.5	< 2.4	<1.5
H-factor	<2.7	<2.9	<3.6
l_i	0.8-1.4	1.2-2.4	0.8-1.2
p(0)/<p>	~1.8-2.5	~1.8-3.5	~4-7

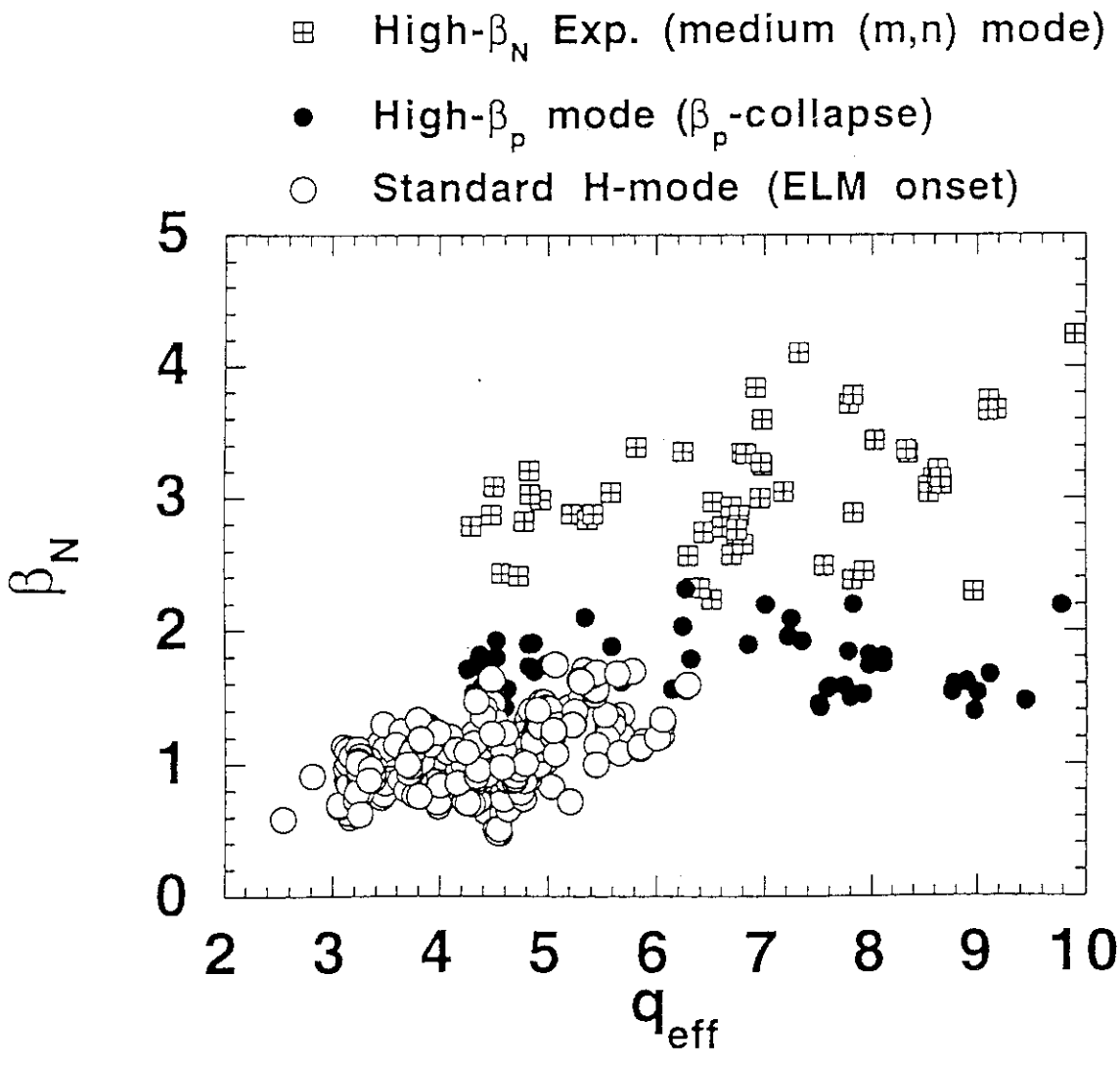

Fig 1:The achieved values of β_N as a function of q_{eff}. In the standard H-mode discharges (opencircles), the obtained β_N-values are lower than 1.8 which is limited by onset of ELMs. In the high-β_N mode discharges (closed circles), the achievable β_N-values are limited by the appearance of the β_p-collapse. In the high β_N experiment (open squares) the pressure driven MHD mode with low(m, n) restricts the β_N-values.

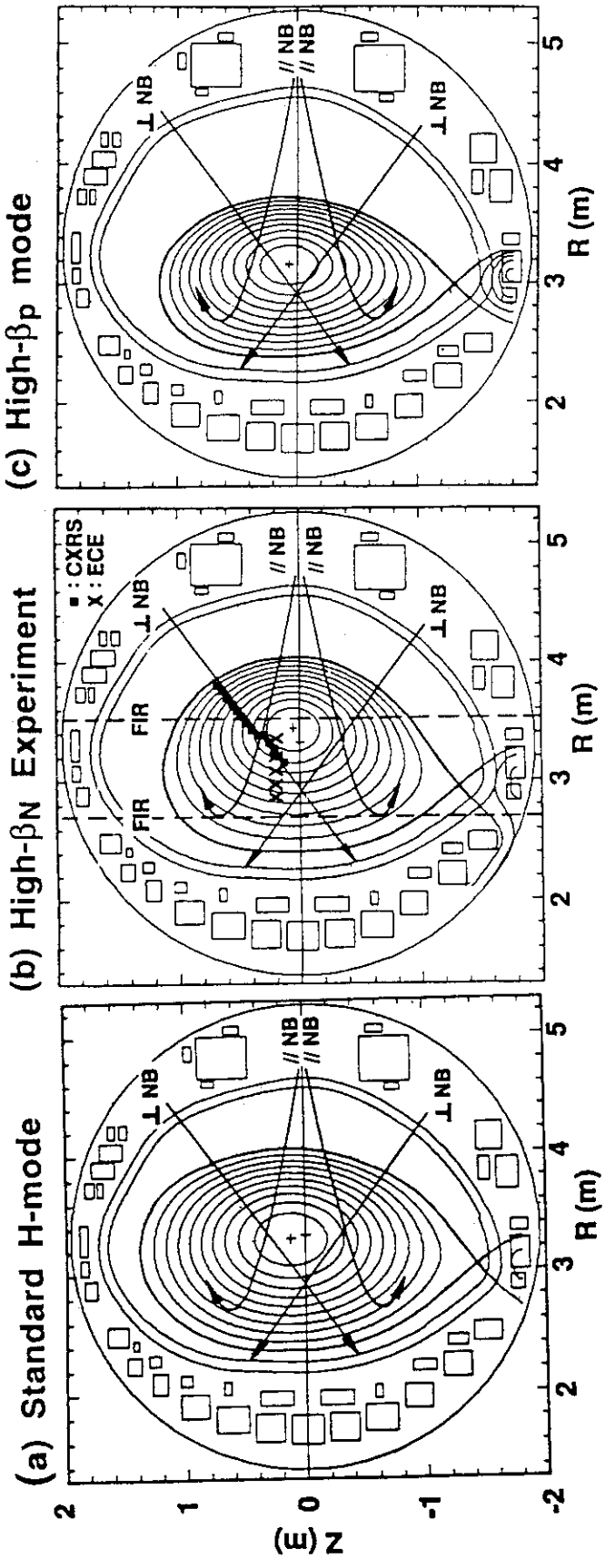

Fig 2:The typical plasma configuration for (a) the standard H-mode, (b)the high β_N experiment and (c) the high- β_p mode.

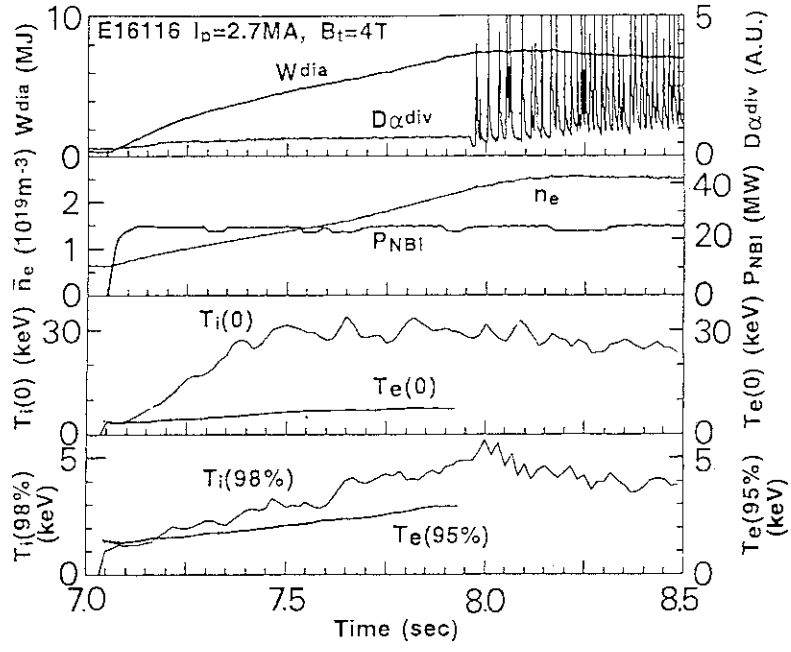

Fig 3:The time evolution of the typical H-mode discharge(E16116).

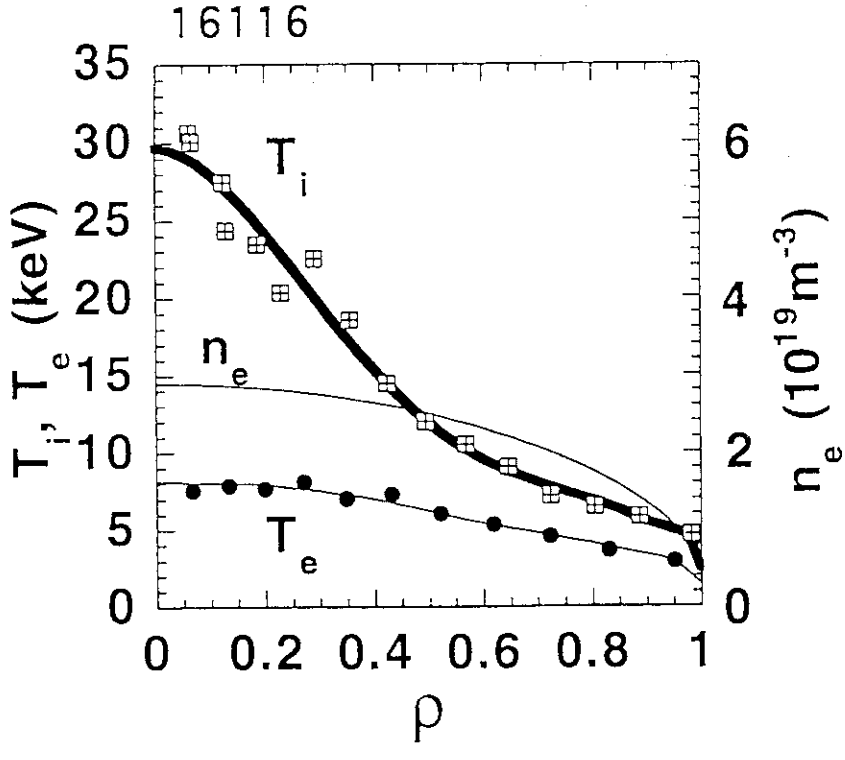

Fig 4:The profiles of T_i, T_e and electron density $\bar{n}_e$ just before the onset of ELMs (t=7.8s of E16116).

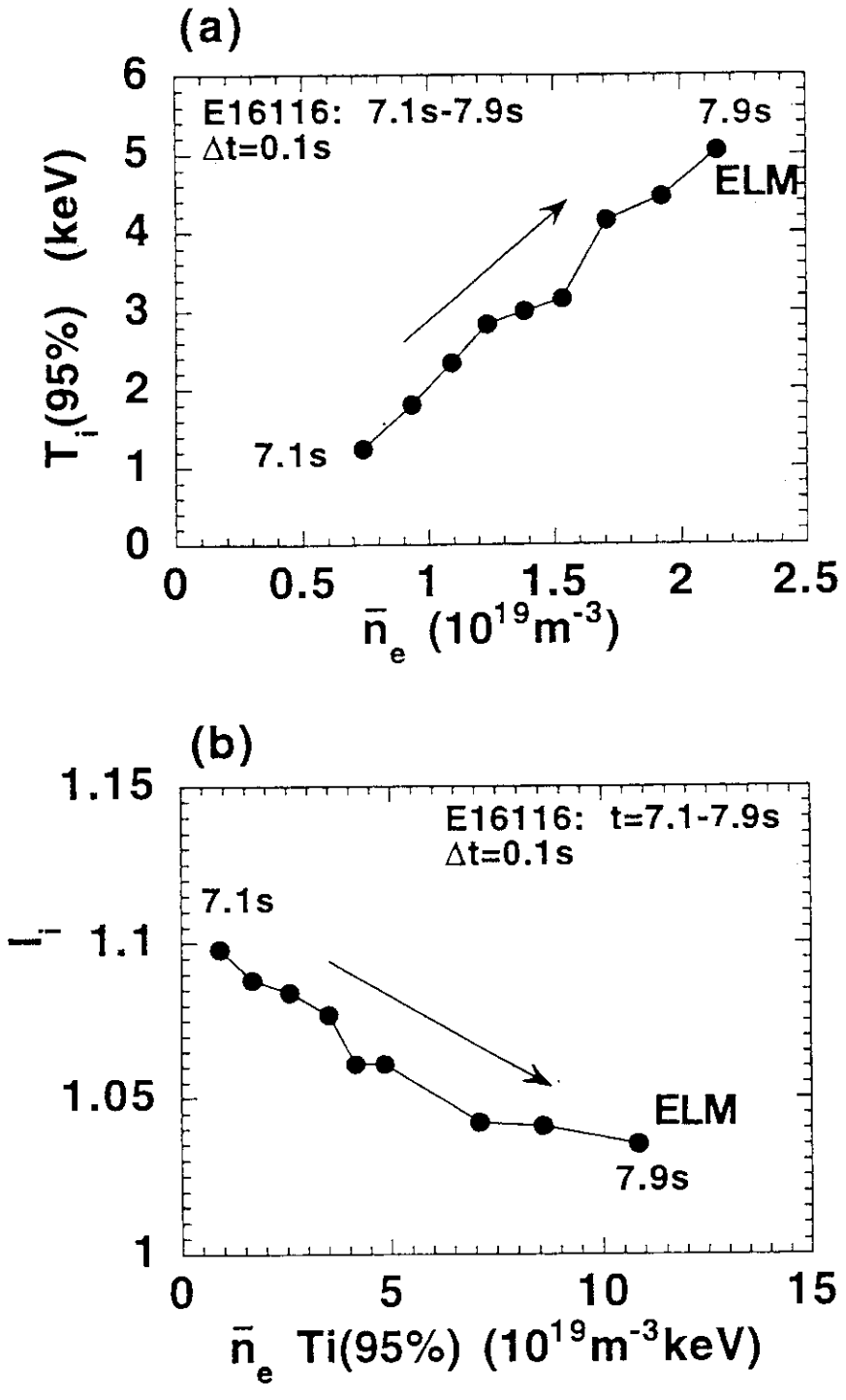

Fig 5:Time evolution of T_i (95%), $\bar{n}_e$ (0.4-0.5a), l_i and $\bar{n}_e$(0.4-0.5a) T_i(95%) from 7.1s (NB turn-on)to 7.9s(ELM onset)for the discharge E16116.(a): The edge plasma in JT-60U H-mode is that the edge temperature increases almost linearly with increasing n_e. (b) With the evolution of H-mode, l_i decreases and $\bar{n}_e$ T_i (95%) increases, and the first ELM appears at $\bar{n}_e$ T_i(95%)$\sim$11x$10^{19}m^{-3}$keV.

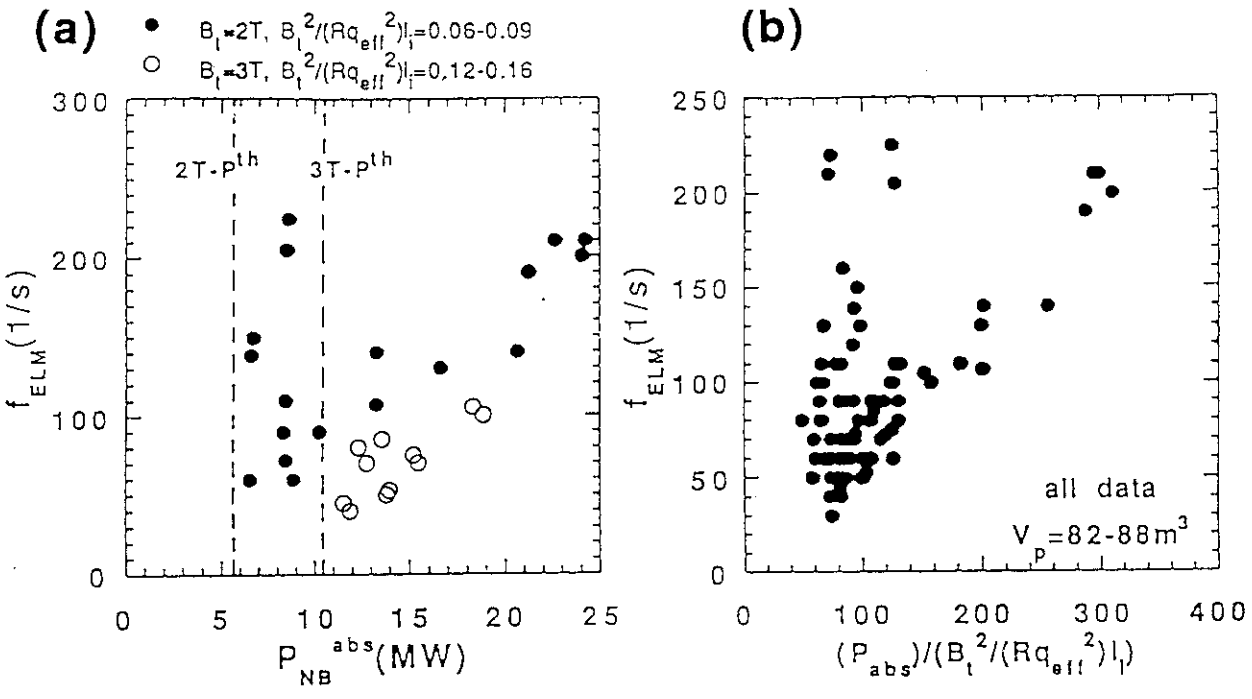

Fig 6:(a): ELM frequency f_{ELM} against absorbed NB power P_{NB}^{abs} for B_t=2T(closed circles) and 3T (open circles) with the plasma volume V_p=82-88m^3. The threshold power P_{abs}^{th} for the L-Htransition is indicated by dashed lines. Both open and closed circles increase almost linearly with P_{NB}^{abs} if P_{NB}^{abs} is high enough. On the other hand, if P_{NB}^{abs} is close to P_{abs}^{th} , there is another group with high f_{ELM} . (b): f_{ELM} increases linearlywith$(P_{NB}^{abs})/((B_t^2/(Rq_{eff}^2))l_i)$ in the first group . In the second group, f_{ELM} ishigh even at low P_{NB}^{abs} .

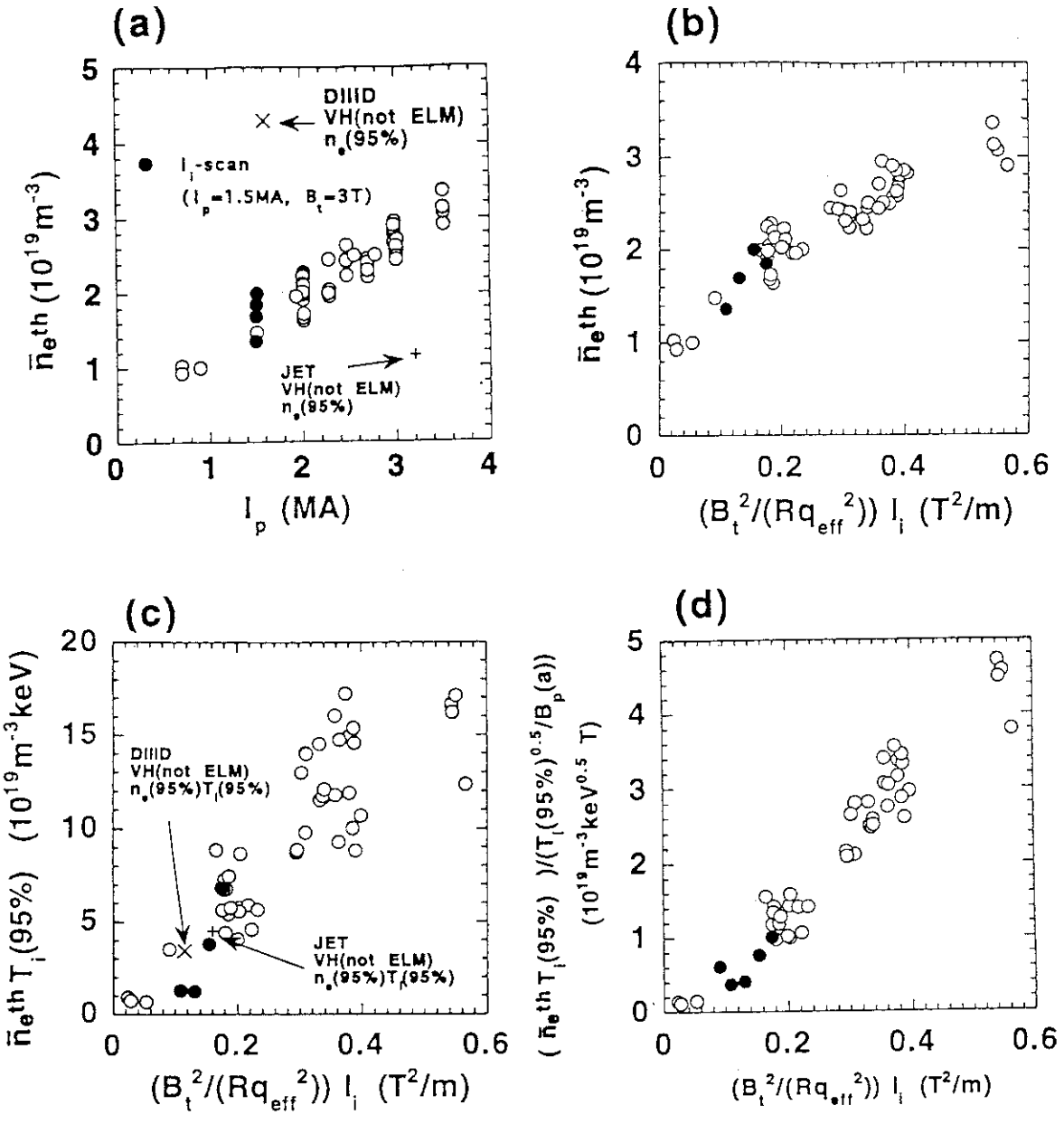

Fig 7:Data at the onset of the first ELM. Open circles indicate the data taken in a wide rangeof I_p (0.7-3.5MA) and B_t (1.5-4T) and closed circles corresponds to the data for a fixed B_t^2 / (Rq_{eff}^2(=0.08-0.11;1.5MA, 3T). (a): The threshold density $\bar{n}_e^{th}$ increases with I_p. (b) : The relationship between $\bar{n}_e^{th}$ and (B_t^2 / (Rq_{eff}^2))I_i. (c): $\bar{n}_e$ (0.4-0.5a) T_i (95%) (a measure of the edge pressure) at the onset of ELMs increases with (B_t^2/(Rq_{eff}^2))I_i.(d): A measure parameter of the edge pressure gradient ($\bar{n}_e^{th}$ T_i (95%))/(T_i (95%)$^{0.5}$/ Bp(a) is clearly proportional to (B_t^2/ (Rq_{eff}^2))I_i. In(a) and (c), data of n_e (95%)and n_e (95%) T_i (95%) for the VH-mode in DIIID and JET reported in Ref. [13] are plotted for comparison. In these VH-mode discharges, n_e (95%) and n_e (95%) T_i (95%) are not limited by appearance of ELMs.

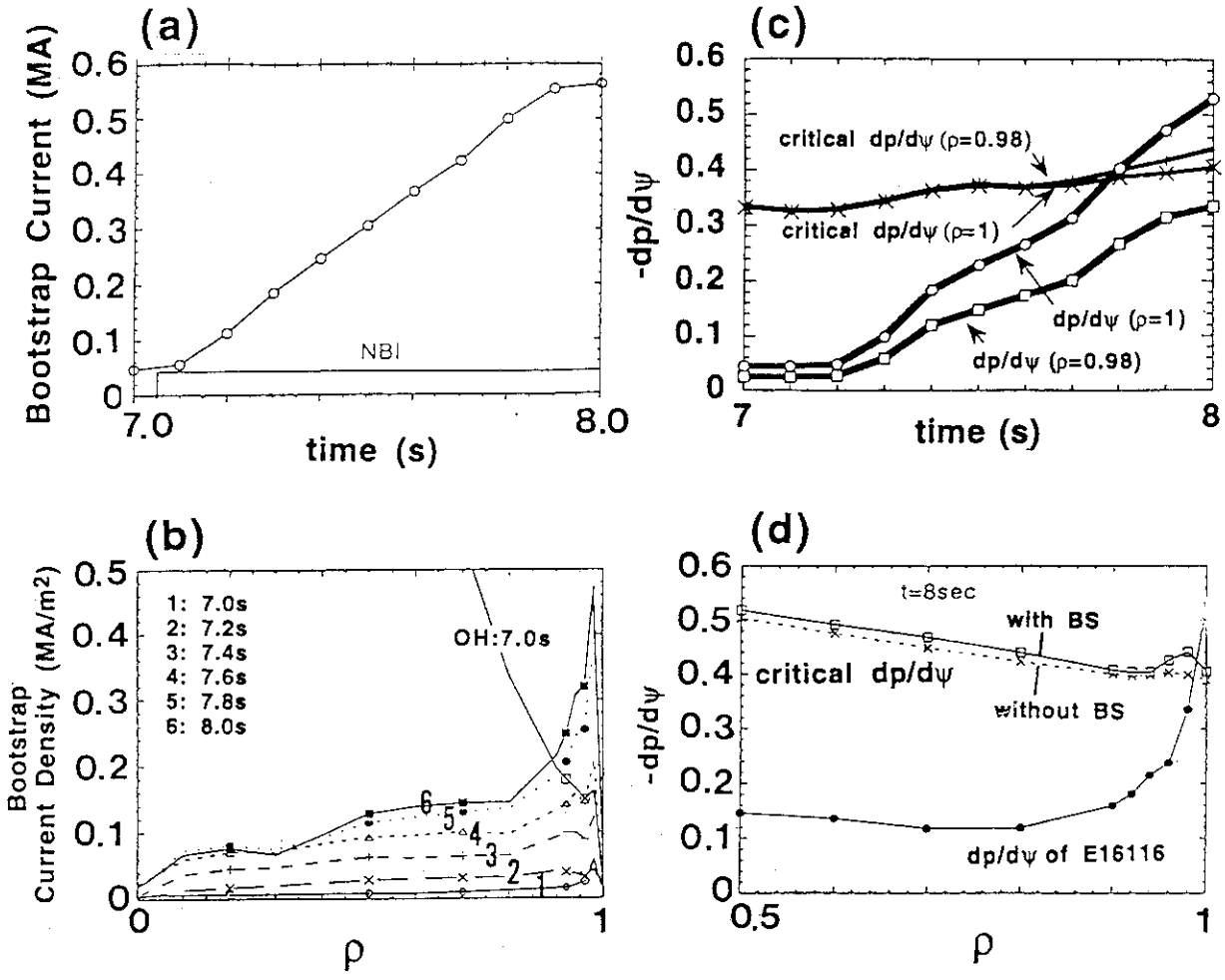

Fig 8:The evolution of the bootstrap current and the stability condition of the high-n ideal ballooning mode for the discharge E16116. (a):Amount of the bootstrap current increases almost linearly until the onset of ELMs. (b) : The evolution of the bootstrap current profile which is highly peaked in the edge region. (c): The evolution of the edge stability condition. Open squares and open circles correspond to the-dp/d Ψ at p=0.98 and p=1, respectively. The critical pressure gradient for the high-n ballooning stability at p=0.98 and p=1 are shown by + and x, respectively. (d) The profiles of the measured pressure gradient and the critical pressure gradient for the ballooning stability. The solid line with open squares and the dotted line are the critical pressure gradient with and without the bootstrap current, respectively.

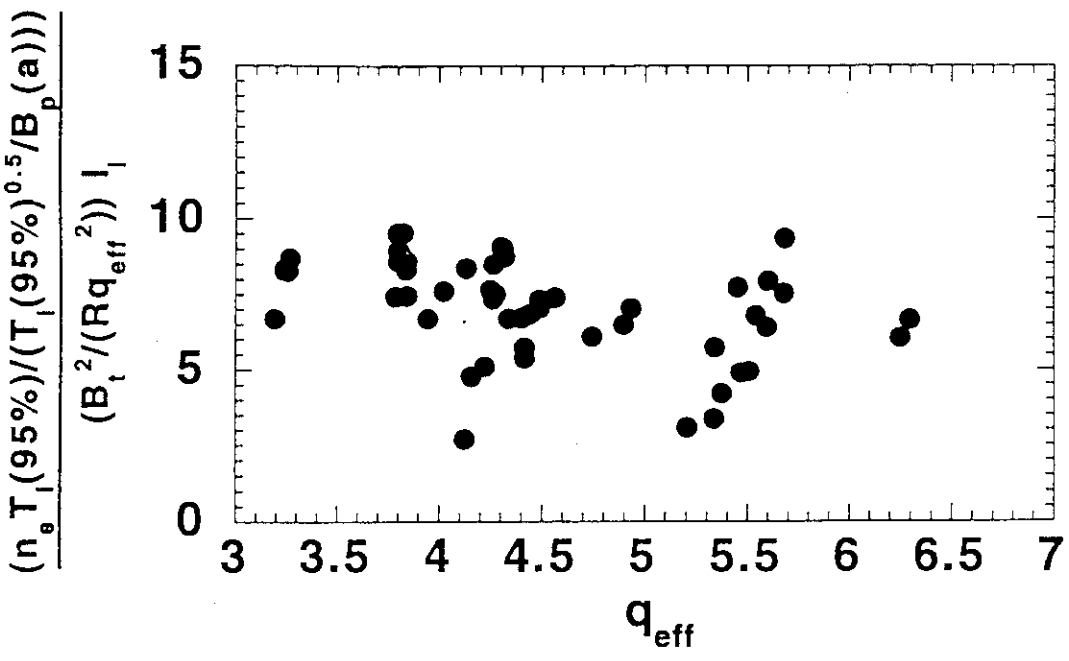

Fig 9:The tangent of Fig.7 (d) $((\bar{n}_e{}^{th}\ T_i\ (95\%))/(\ T_i\ (95\%)^{0.5}/Bp(a)))/(\ B_t{}^2/Rq_{eff}{}^2))l_i))$ as a function of q_{eff} . Although the values are nearly constant in a wide range of q_{eff} , the lower boundary of the data has fine structure depending on q_{eff} in particular when q_{eff} is around integer.